

Dynamics of charge transport and recombination in ZnO nanorod array dye-sensitized solar cells

Alex B. F. Martinson, James E. McGarrah, Mohammed O. K. Parpia and Joseph T. Hupp*

Received 24th July 2006, Accepted 4th September 2006

First published as an Advance Article on the web 13th September 2006

DOI: 10.1039/b610566a

Intensity modulated photovoltage and photocurrent spectroscopies reveal that photoanodes based on nanorod arrays exhibit dramatically faster electron transport while retaining similar electron lifetimes (recombination times) compared to standard photoanodes assembled from colloidal nanoparticles.

Introduction

Dye-Sensitized Solar Cells (DSSCs) comprise an increasingly attractive alternative photovoltaic technology.^{1,2} These photoelectrochemical cells use molecular dyes to sensitize high-area, wide band gap semiconductor oxide anodes built on conductive glass. Typically, a liquid electrolyte scavenges the residual hole on the chromophore and shuttles it to a Pt-coated counter electrode, where the circuit is completed. Alternatively, a solid-state (molecular or polymeric) hole scavenger/conductor can be used.³ The most efficient DSSCs offer light-to-electrical energy conversion efficiencies of 11%, but suffer from relatively poor photovoltages due to the overpotential needed to drive the dye regeneration (*i.e.* hole scavenging) reaction. Furthermore, they show less than optimal photocurrents due to insufficient light collection in the red part of the visible spectrum.⁴

Compared to the most efficient nanocrystalline TiO₂ photoanodes, devices with ZnO electrodes show significantly lower conversion efficiencies (<4%).^{5–7} Yet ZnO DSSCs continue to be actively investigated due to the ease with which alternative and potentially superior high-area semiconductor morphologies may be fabricated. Particularly interesting are nanorod arrays.^{8–11} Compared with standard photoanodes based on sintered nanocrystalline particles, a nanorod photoanode should show significantly faster electron transport, owing to a more direct path to the conductive glass electrode combined with fewer sites for trapping electrons.⁸

If one can avoid simultaneously accelerating reverse electron transfer from the photoelectrode to the dye or regenerator, speeding up electron transport provides opportunities for enhancing the performance of DSSCs in several ways. The useful thickness of a photoanode is determined by its effective electron diffusion length,

$$L_n = (D_n \tau_n)^{1/2} \quad (1)$$

where D_n is the effective diffusion coefficient for the electron

within the photoelectrode and τ_n is the survival time of the electron with respect to recombination with the oxidized dye or regenerator. DSSCs employing solid-state hole-conductors in particular suffer from an L_n less than the thickness required to absorb the majority of incident light.¹² The result is low Light Harvesting Efficiency (LHE) or poor charge collection efficiency (η_c), both of which limit the Incident Photon-to-Current Efficiency (IPCE) according to

$$\text{IPCE} = \text{LHE} \cdot \phi_{\text{inj}} \cdot \eta_c \quad (2)$$

where ϕ_{inj} is the efficiency of electron injection from the excited dye into the semiconductor framework. Faster transport, therefore, can increase L_n and thus increase LHE and photocurrent.

In the most efficient liquid electrolyte DSSCs, L_n is already greater (at most wavelengths) than the thickness required to collect most of the incident photons. Here, the result of faster transport (larger D_n) would be to make the cells tolerant to faster recombination dynamics (shorter τ_n (eqn (1)); recall that the electron collection efficiency is a measure of the competition between transport and recombination). In principle, faster redox shuttles could then be employed. As dye regeneration by inherently faster shuttles need not be accelerated by large overpotentials, this change could directly address the problem of low photovoltage that has plagued DSSCs since their inception.

Work by Law and co-workers establishes that electron transport within isolated ZnO nanorods is indeed rapid.⁸ However, this important earlier study does not directly address the dynamics of transport within operating solar cells, nor does it examine recombination dynamics. While the current article was in review, a conceptually-related report was published by Galoppini *et al.* They observed similar charge transport dynamics for ZnO nanorods grown by MOCVD on Si substrates and sensitized by porphyrins.¹³

Here, we report on a comparison of transport dynamics and recombination dynamics for sintered nanocrystalline particle *versus* nanorod array electrodes of zinc oxide within operating DSSCs featuring the Grätzel group's ruthenium chromophore, N719. Average electron transport times, τ_d , were evaluated by Intensity Modulated Photocurrent Spectroscopy (IMPS), while average recombination times were determined by Intensity Modulated photoVoltage Spectroscopy (IMVS).^{14–17} The transport time and effective diffusion coefficient are inversely related:

$$\tau_d = \text{constant} \bullet L^2/D_n \quad (3)$$

2145 Sheridan Rd., Evanston, IL 60208, USA. E-mail: j-hupp@northwestern.edu; Fax: 1 847 467 1425; Tel: 1 847 467 1425

where L is the thickness of the photoelectrode, and the magnitude of the constant (typically between 0.25 and ~ 0.4) depends on factors such as the uniformity (or otherwise) of carrier generation through the thickness of the electrode.

Since our objective was to understand and compare dynamics rather than maximize cell efficiency, optically dilute cells were employed. These provide for simplified behavior by allowing for uniform illumination/light-collection through the full depth of the photoelectrode. Using such cells, we find that nanorod geometries clearly do offer substantial dynamical advantages relative to nanocrystalline particulate (np) geometries.

Results and discussion

Scanning Electron Microscopy (SEM) images of a sintered np network (Fig. 1a) and a nanorod array (Fig. 1b) illustrate the differences in photoelectrode morphology. The sintered network consists of 20–200 nm diameter particles with similar size pores. The array largely comprises aligned rods of average length 4500 nm and of average diameter 150 nm, yielding an average aspect ratio of ~ 30 . Previous reports have shown that ZnO rods prepared by similar hydrothermal methods are highly crystalline.^{10,18,19} In the experiments described below, photoelectrode thicknesses have been approximately matched so that transport times can be directly compared and uncertainties associated with conversion to diffusion coefficients can be avoided.

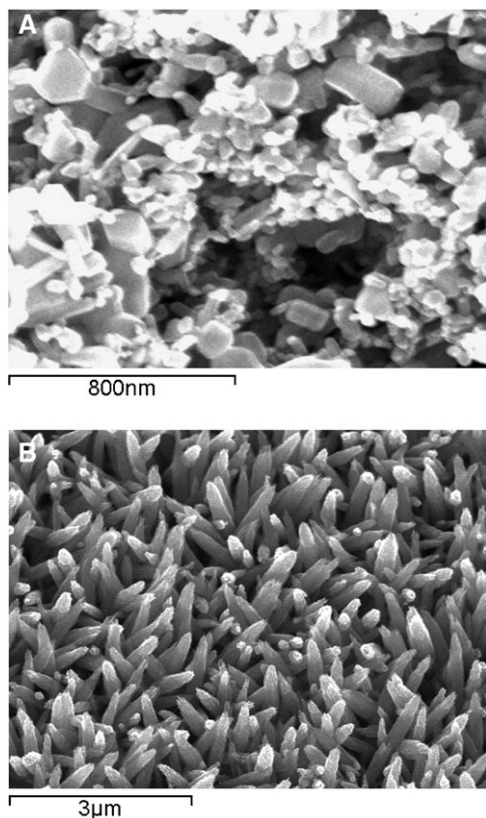


Fig. 1 Scanning electron micrograph of (a) nanoparticulate ZnO photoelectrode and (b) ZnO nanorod array photoelectrode.

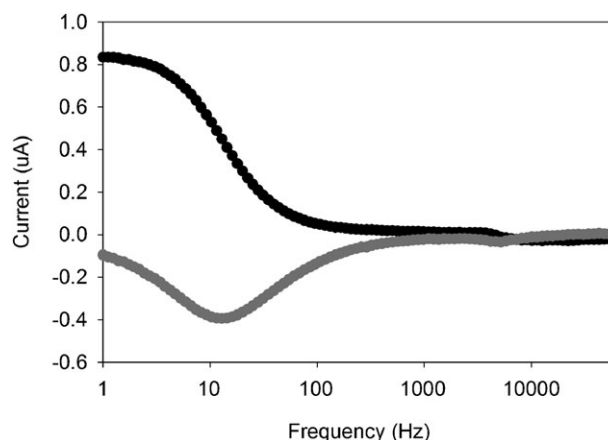


Fig. 2 Real (black) and imaginary (grey) components of the photo-modulated current for a $3.8 \mu\text{m}$ thick nanoparticle electrode as a function of modulation frequency.

The protocol in photomodulation experiments is to systematically (sinusoidally) vary a small fraction of the light intensity, thereby systematically varying the number of charge carriers (*i.e.* injected electrons). The external electrical response—either the photocurrent at short circuit (IMPS) or photovoltage at open circuit (IMVS)—is then monitored as the modulation frequency is increased.^{14,15} At some point the electrical response begins to lag behind the optical perturbation, indicating rate-limiting dynamics for either charge transport or recombination.

Fig. 2 shows real and imaginary components of the photo-modulated current for a $3.8 \mu\text{m}$ thick np electrode as a function of modulation frequency, $f (= \omega/2\pi)$. The average transport time may be estimated from the minimum angular frequency in the imaginary plot:¹⁴

$$\tau_d = \omega_{d,\min}^{-1} \quad (4)$$

The value obtained is 12 ms.

Fig. 3 shows the results of the same type of experiment, but now for a $4.5 \mu\text{m}$ thick nanorod array electrode. The striking feature is a shift of two orders of magnitude toward a higher characteristic lag frequency, indicating that τ_d is two orders of magnitude shorter and the transport dynamics are two orders of magnitude faster for electrons within the nanorod array electrode. Closer examination shows that the current *versus* frequency plots deviate slightly from the expected sigmoidal and (approximately) Gaussian lineshapes for the real and imaginary components, respectively. Distortions are expected when transport becomes fast enough that other impedance elements, such as the cell series resistance (R) and the photoelectrode capacitance (C), limit the dynamical response of the photocell. To correct for these effects, the real and imaginary IMPS signals were divided by the complex attenuation function, $A(\omega)$:¹⁷

$$A(\omega) = \frac{1 - i\omega RC}{1 + \omega^2 R^2 C^2} = \frac{1}{1 + i\omega RC} \quad (5)$$

As shown in Fig. 3 (open symbols), the correction shifts the minimum frequency still higher, yielding an average transport time of $74 \mu\text{s}$ and indicating that electrons are transported

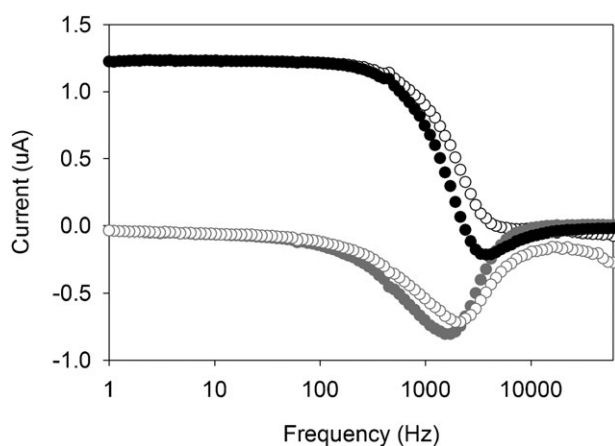


Fig. 3 Real (black) and imaginary (grey) components of the photo-modulated current for a 4.5 μm thick nanorod electrode as a function of modulation frequency. Open circles show the current corrected for RC attenuation (eqn (4)), where R and C take typical literature values, 15Ω and $30\ \mu\text{F cm}^{-2}$.

~ 160 times more rapidly through the nanorod array electrode than through the np electrode. If corrections are made for the slight mismatch in thickness (transport is slower through thicker electrodes; see eqn (3)), the difference in transport dynamics is even greater: ~ 220 -fold.

The dynamics of recombination can be evaluated from similar plots of real or imaginary contributions to the modulated photovoltage under open-circuit conditions.¹⁴ Equating the observed angular frequency at the minimum imaginary photovoltage with τ_n^{-1} , we obtained average recombination times of 47 and 170 ms, respectively, for the np and nanorod array electrodes at the light intensity used in Fig. 2 and 3. These findings are significant because they clearly show that the enhanced transport obtained with the nanorod array geometry does not come at the expense of similarly enhanced recombination dynamics. Indeed, recombination is *slower* for the nanorod array geometry than the np geometry. (The difference may be due, in part, to differences in total electrode area. In general, recombination accelerates when the electrode area increases. While we have not been able to quantify the difference, the areas of np electrodes of a given thickness almost certainly are greater than those of nanorod electrodes of the same thickness.)

Fig. 4 shows the dependence of dynamics on mean light intensity. The np electrode behaves as expected: charge transport and recombination both accelerate with increasing light flux, but their ratio remains essentially constant ($\tau_d/\tau_n \approx 3.5$). Thus, reasonably efficient charge collection is achievable with $L = 3.8\ \mu\text{m}$, but should be much less so with an optically thick electrode (*e.g.* L greater than, say, 10 or 15 μm).

For the nanorod array electrode, the dynamics of recombination are similarly intensity dependent. The observed faster recombination at higher light intensity is expected because the local concentrations of both reactants (injected electrons and triiodide) are increased. Surprisingly, however, the dynamics of electron transport are insensitive to photon flux. The more typically observed enhancement of transport dynamics with increasing light flux has usually been explained by assuming

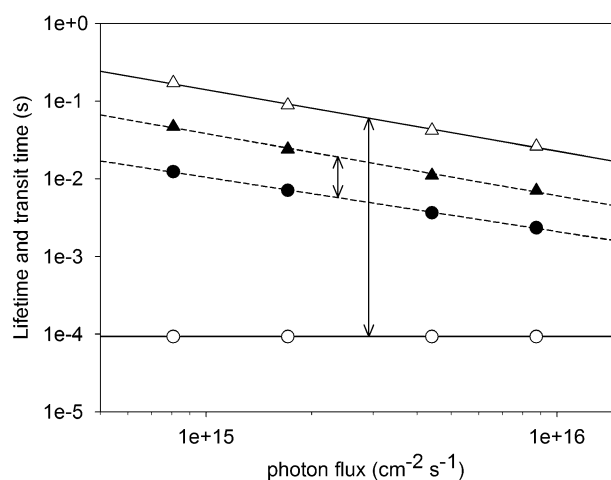


Fig. 4 Electron lifetime (triangles) and average transit time (circles) over a range of illumination intensities. Arrows highlight the difference between τ_n and τ_d for nanoparticle (filled symbol) and nanorod (open symbol) devices.

that many electron traps exist and that they are distributed over a range of energies. Transport is thought to occur by a multistep process: occasional Boltzmann-governed thermal detrapping, followed by rapid movement through the conduction band until trapping occurs once again and the electron is largely immobilized.²⁰ At low light intensities, only the lowest energy traps are filled. At higher intensity, more electrons are present so more traps are filled and a smaller energy difference exists between the highest-energy filled traps and the conduction band. The smaller the energy difference, the more likely that transient detrapping (and electron transport) will occur. Phenomenologically, this behavior would be manifest as an increase in the effective diffusion coefficient (decrease in transport time) with increasing light intensity.

That this behavior is *not* seen for the nanorod array electrode suggests either that all traps are filled, even at the lowest light intensity, or that traps are clustered around a single energy rather than being widely distributed in energy. (Typically an exponential distribution has been assumed.) Alternatively, a bottleneck unrelated to transport through the nanorod could conceivably exist. If so, then the measured transport times are only lower-limit estimates of the nanorod dynamics, *i.e.* the true times could be shorter and the true dynamics faster than indicated in Fig. 4.

From Fig. 4, the measured ratio of recombination time to transport time for the nanorod electrode varies from 280 to 1850. If the results are extrapolated to the number of photons incident in the absorbing range of the dye under AM 1.5 illumination, the ratio becomes ~ 64 —or about 18 times that seen with the np electrode geometry. Thus, nanorod array cells should be capable of sustaining efficient charge collection over much greater thicknesses than nanoparticle-based cells.

Finally, for completeness, we show in Fig. 5 plots of photocurrents *versus* photovoltages for the two types of cells. We emphasize, however, that comparisons are complicated because differences in real area and in LHE for the two types of cells. Nevertheless, the observation of comparable photocurrent from the nanorod cell relative to the np cell, despite

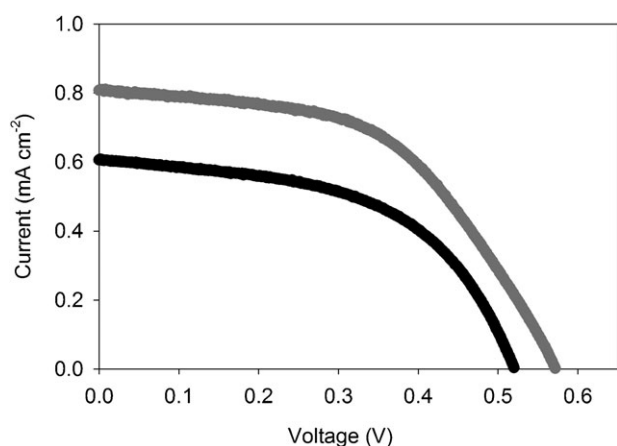


Fig. 5 Plots of current *versus* voltage for np (grey) and nanorod (black) cells under white light at approximately 1 sun. Note that dye loadings and, therefore, LHEs are low in both cases. Note also that the real area of the nanorod cell is significantly less than that of the np cell.

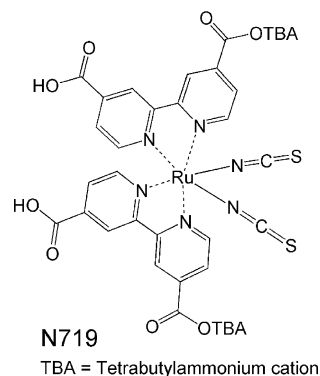
significantly lower LHE for the nanorod cell, points to more effective charge collection for this cell.

In summary, photomodulation experiments with dye-sensitized ZnO solar cells show that electron transport is tens to hundreds of times faster in nanorod array electrodes than in nanocrystalline particulate electrodes. Recombination, on the other hand, is slightly slower. Taken together, these findings support the contention that nanorod geometries are likely to provide very substantial dynamical advantages in operating dye-sensitized solar cells.

Experimental

All photoelectrodes were prepared on fluorine-doped tin oxide coated glass ($8 \Omega \text{ cm}^{-2}$). Nanocrystalline ZnO films were prepared using a commercial ZnO powder (Aldrich, nanopowder, 99.999%) according literature reports.²¹ A ZnO slurry was made by mixing ZnO powder and hydroxy propyl cellulose in distilled water followed by evaporation until the ZnO content reaches 6 wt%. Nanorod ZnO films were prepared *via* a two-step procedure similar to the various literature reports of ZnO nanorod arrays on conductive glass.^{10,18,19} Briefly, RF magnetron sputtering of ZnO served to deposit a reproducible seeding surface upon which nanorod growth initiates. Growth of the rods was accomplished by immersing the slides in a 0.2 mM aqueous solution of $\text{Zn}(\text{NO}_3)_2$ adjusted to pH 10.3 with aqueous ammonia (28 wt%) at 65 °C for 6 h in a sealed vessel. This typically yielded nanorod coatings showing a single morphology across the entire $15 \times 25 \text{ mm}$ slide that are $4.5 \pm 0.2 \mu\text{m}$ high and 100–200 nm in diameter. Thicker samples were obtained by re-immersing the electrodes in a fresh growth solution, similar to previously reported methods.^{10,19} Active areas were patterned with nail polish. The remainder of the nanorod sample was dissolved in 10 wt% HCl (aq). The nail polish was washed away with acetone. The samples were sintered in air at 400 °C for 0.5 h and cooled to 100 °C. The warm slides were submerged in N719 dye, $(\text{Ru}(\text{mpdcb})_2(\text{SCN})_2) \cdot (\text{tBu}_4\text{N})_2$, where mpdcb is monoprotonated 4,4'-dicarboxy-2,2'-bipyridine), for 24 h. Film thick-

nesses were measured on a Tencor P10 profilometer. SEM images were collected on a Hitachi S-4500 cFEG SEM.



Cells were assembled according to literature procedures and infiltrated with an electrolyte solution containing 0.60 M butylmethylimidazolium iodide, 0.03 M I_2 , 0.10 M guanidinium thiocyanate and 0.50 M *tert*-butylpyridine in a mixture of acetonitrile and valeronitrile (85 : 15). The active areas of np and nanorod array devices were $\sim 0.4 \text{ cm}^2$ and $\sim 0.7 \text{ cm}^2$, respectively. Completed cells were illuminated by an array of high intensity blue LEDs (Nichia Corporation, 471 nm) driven by a Solartron 1260 Frequency Response Analyzer (FRA). The dc light intensity was varied from 0.34–3.70 mW cm^{-2} by changing the current through the LEDs. A 10% ac modulation was also applied to the LEDs *via* the FRA. For IMVS, the amplitude and phase shift of the modulated open-circuit photovoltage relative to the modulated illumination was measured directly by the FRA. For IMPS, the modulated short-circuit photocurrent was measured by a Solartron 1286 electrochemical interface and passed as a voltage to be read by the FRA. Data acquisition was performed using the GPIB output of the FRA attached to a personal computer.

Acknowledgements

We gratefully acknowledge support from BP Solar and from the U. S. Department of Energy, Basic Energy Sciences Program (Grant No. DE-FG02-87ER13808). ABFM thanks the Link Foundation and the Electrochemical Society for graduate fellowships. MOKP acknowledges support from the Northwestern University Nanoscale Science and Engineering Center.

References

- 1 M. Grätzel, *Nature*, 2001, **414**, 338–344.
- 2 M. Grätzel, *MRS Bull.*, 2005, **30**, 23–27.
- 3 U. Bach, D. Lupo, P. Comte, J. E. Moser, F. Weissörtel, J. Salbeck, H. Spreitzer and M. Grätzel, *Nature*, 1998, **395**, 583–585.
- 4 M. K. Nazeeruddin, F. DeAngelis, S. Fantacci, A. Selloni, G. Viscardi, P. Liska, S. Ito, B. Takeru and M. Grätzel, *J. Am. Chem. Soc.*, 2005, **127**, 16835–16847.
- 5 E. Hosono, S. Fujihara, I. Honna and H. S. Zhou, *Adv. Mater.*, 2005, **17**, 2091–2094.
- 6 K. Kakiuchi, E. Hosono and S. Fujihara, *J. Photochem. Photobiol., A*, 2006, **179**, 81–86.
- 7 I. Bedja, P. V. Kamat, X. Hua, A. G. Lappin and S. Hotchandani, *Langmuir*, 1997, **13**, 2398–2403.
- 8 M. Law, L. E. Greene, J. C. Johnson, R. Saykally and P. D. Yang, *Nat. Mater.*, 2005, **4**, 455–459.

-
- 9 K. S. Kim, Y. S. Kang, J. H. Lee, Y. J. Shin, N. G. Park, K. S. Ryu and S. H. Chang, *Bull. Korean Chem. Soc.*, 2006, **27**, 295–298.
 - 10 Y. F. Gao and M. Nagai, *Langmuir*, 2006, **22**, 3936–3940.
 - 11 P. Ravirajan, A. M. Peiro, M. K. Nazeeruddin, M. Graetzel, D. D. C. Bradley, J. R. Durrant and J. Nelson, *J. Phys. Chem. B*, 2006, **110**, 7635–7639.
 - 12 J. Kruger, R. Plass, M. Gratzel, P. J. Cameron and L. M. Peter, *J. Phys. Chem. B*, 2003, **107**, 7536–7539.
 - 13 E. Galoppini, J. Rochford, H. Chen, G. Saraf, Y. Lu, A. Hagfeldt and G. Boschloo, *J. Phys. Chem. B*, 2006, **110**, 16159–16161.
 - 14 L. M. Peter and K. G. U. Wijayantha, *Electrochim. Acta*, 2000, **45**, 4543–4551.
 - 15 G. Schlichthorl, S. Y. Huang, J. Sprague and A. J. Frank, *J. Phys. Chem. B*, 1997, **101**, 8141–8155.
 - 16 F. Cao, G. Oskam, G. J. Meyer and P. C. Searson, *J. Phys. Chem.*, 1996, **100**, 17021–17027.
 - 17 L. Dloczik, O. Ieperuma, L. Lauermann, L. M. Peter, E. A. Ponomarev, G. Redmond, N. J. Shaw and I. Uhlendorf, *J. Phys. Chem. B*, 1997, **101**, 10281–10289.
 - 18 K. Govender, D. S. Boyle, P. B. Kenway and P. O'Brien, *J. Mater. Chem.*, 2004, **14**, 2575–2591.
 - 19 L. E. Greene, M. Law, D. H. Tan, M. Montano, J. Goldberger, G. Somorjai and P. D. Yang, *Nano Lett.*, 2005, **5**, 1231–1236.
 - 20 A. J. Frank, N. Kopidakis and J. van de Lagemaat, *Coord. Chem. Rev.*, 2004, **248**, 1165–1179.
 - 21 N. G. Park, M. G. Kang, K. M. Kim, K. S. Ryu, S. H. Chang, D. K. Kim, J. van de Lagemaat, K. D. Benkstein and A. J. Frank, *Langmuir*, 2004, **20**, 4246–4253.